Atomic-Scale Visualization of Antisite Defects in $LiFePO_4$

Sung-Yoon Chung,[1,2,*] Si-Young Choi,[3,4,†] Takahisa Yamamoto,[5,6] and Yuichi Ikuhara[3,6]

[1]*Department of Materials Science and Engineering, Inha University, Incheon 402-751, Korea*
[2]*Nalphates LLC, Wilmington, Delaware 19801, USA*
[3]*Institute of Engineering Innovation, The University of Tokyo, Tokyo 113-8656, Japan*
[4]*Korea Institute of Materials Science, Changwon 641-831, Korea*
[5]*Department of Advanced Materials Science, The University of Tokyo, Tokyo 113-8656, Japan*
[6]*Nanostructures Research Laboratory, Japan Fine Ceramics Center, Nagoya 456-8587, Japan*

(Received 13 September 2007; published 26 March 2008)

We visualize the antisite exchange defects in $LiFePO_4$ crystals with an ordered olivine structure by using annular dark-field scanning transmission electron microscopy (STEM). A recognizable bright contrast is observed in some of the Li columns of STEM images in a sample annealed at a lower temperature, which directly demonstrates the disordered occupations by Fe atoms. Furthermore, such exchange defects appear to be locally aggregated rather than homogeneously dispersed in the lattice, although their overall concentration is fairly low. The present study emphasizes the significance of atomic-level observations for the defect distribution that cannot be predicted by macroscopic analytical methods.

DOI: 10.1103/PhysRevLett.100.125502 PACS numbers: 61.72.Ff, 61.72.J−, 68.55.Ln, 82.45.Xy

Olivine-type minerals, some of which are major constituents of Earth's upper mantle [1], have been extensively studied due to their geophysical significance and have been used as insulators and refractories when outstanding thermochemical stability is required [2]. Among all of the thermodynamic variables, the point defects in these minerals, such as cation vacancies, antisite defects, and hydrogen impurities, are known to critically affect the physical properties of the minerals including electrical conduction, ionic diffusion, and deformation behavior [3]. Determination of the cation partitioning between the two different octahedral interstitial sites (edge-sharing "$M1$" and corner-sharing "$M2$" sites) in the unit cell has been a particularly important issue for understanding crystallographic stability under specific circumstances [4,5]. Thus far, most of the analytical investigations on the antisite exchange were largely based on neutron powder diffraction. However, such a macroscopic diffraction approach can only show the overall simple distribution of metal cations between the two sites through the refinement of obtained spectra. In this regard, direct atomic-level observation of the antisite defects is essential to precisely probe the local distribution of the defects in the crystal lattice, especially when the degree of the exchange is quite low.

The recent development of aberration-corrected scanning transmission electron microscopy (STEM) [6,7] along with progress in the Z-contrast technique [8–13] not only enable the achievement of sub-angstrom resolution for imaging [10], but also allow the probing of zero-dimensional point defects in crystals to be facilitated with enhanced spatial localization of the intensity of the electron beam [11,13]. Taking $LiFePO_4$, the mineral name of which in nature is triphylite, with cation ordering, as an example for investigation of the cation exchange in an ordered olivine structure, we directly visualized the antisite defects in the lattice at an atomic scale by aberration-corrected high-angle annular dark-field (HAADF)-STEM. In addition, the defects in the $LiFePO_4$ crystal were observed not to be distributed homogeneously, but to be fairly localized when annealed at 600 °C. While some of the olivine silicates show an increase in cation intermixing between the two different octahedral M sites as the temperature increases above 600 °C [for instance, $MnMgSiO_4$ and $MnFeSiO_4$ (Ref. [5])], we found that such disordered defects in $LiFePO_4$ crystals were scarcely detected during the STEM analysis when annealed at a higher temperature, demonstrating a remarkably high degree of ordering.

$LiFePO_4$ samples were prepared using high-purity lithium carbonate, iron oxalate dihydrate, and ammonium dihydrogenphosphate [14]. A small amount (2 mol%) of potassium carbonate was also added as a flux. A stoichiometric powder mixture of the starting materials was calcined at 350 °C for 5 h in Ar. The calcined amorphous powders were fired again for 5 h at 600 and 800 °C, respectively, to obtain fine crystalline particles for the neutron powder diffraction analysis. Dense pellets pressed with the calcined powder for STEM observation were also sintered at 600 and 800 °C for 5 h in the same Ar atmosphere. The neutron powder diffraction measurement was performed using a neutron source with a wavelength of 1.8367 Å. The diffraction data were collected at room temperature over a scanning range of $0° < 2\theta < 160°$ at a step of 0.05°. Rietveld refinement for structural parameters and data fitting was also carried out using the General Structure Analysis System. The occupation factors of Li and Fe sites were taken as main variables during the data fitting.

Atomic-resolution Z-contrast images were taken in JEM-2100F (JEOL, Japan) at 200 kV with a spherical aberration corrector (CEOS, Germany). The optimum

size of the electron probe was ~1.2 Å. The collection semiangles of the HAADF detector were adjusted from 73 to 195 mrad in order to use large-angle elastic scattering of electrons for clear Z-sensitive images. The thickness of the observed regions in each sample was less than 15 nm when measured from the intensity ratio between the first plasmon-loss and the zero-loss peaks in the electron energy loss spectra. Image simulations were performed using the multislice method. The intensity in ADF images was calculated by summing up the scattered electrons with collection semiangles of 60 to 200 mrad.

As illustrated in the inset of Fig. 1, Li [green (or light gray) sphere] and Fe [red (or gray) sphere] are located in the $M1$ and $M2$ sites [14,15], respectively, forming an ordered orthorhombic olivine structure in a space group of $Pnma$. We first performed high-resolution neutron diffraction analysis using $LiFePO_4$ powder samples synthesized at 600 °C to examine the overall occupation factor in each octahedral M site. Figure 1 compares the measured neutron diffraction pattern and its refined result, showing good agreement between the two patterns. The occupation factors of the Li and Fe sites were calculated to be 0.989 and 0.993, respectively, during the data fitting (see Table S1 in the supplementary information) [16]. Thus, based on this refinement result, we can estimate that the concentration of the antisite defects in $LiFePO_4$ is approximately 1% at 600 °C. When using a sample annealed at 800 °C for the same analysis, however, we obtained higher occupation factors: 0.999 for Li sites and 0.996 for Fe sites (see Fig. S1 and Table S2 in the supplementary information) [16]. Consequently, the present neutron diffraction reveals that the formation of the antisite exchange in $LiFePO_4$ is suppressed with increasing the temperature.

Such a well-ordered crystal structure was directly confirmed by HAADF imaging. Figure 2 shows a raw HAADF-STEM image [Fig. 2(b)] in the [010] projection of a $LiFePO_4$ crystal annealed at 600 °C together with an illustration of the atomic arrangement in the unit cell with the same orientation [Fig. 2(a)]. For direct comparison, the two-dimensional atom arrays are superimposed on the STEM image. The inset in Fig. 2(b) also shows a simulated HAADF image for a unit cell. Because Li [green (or light gray)] is too light to be imaged (even lighter than carbon), each atom column for Li has no contrast at all, which is in accord with the simulated image. The periodically arrayed bright spots in Fig. 2(b) thus directly represent each Fe-P column combined as one single image feature. Fe and P are ~1.26 Å apart from each other in the two-dimensional projection, a distance which might be far enough for the Fe and P columns to be resolved as independent intensities in aberration-corrected STEM. However, since the two atoms are not located on the same plane perpendicular to the b axis, as three-dimensionally shown in Fig. 2(a), the

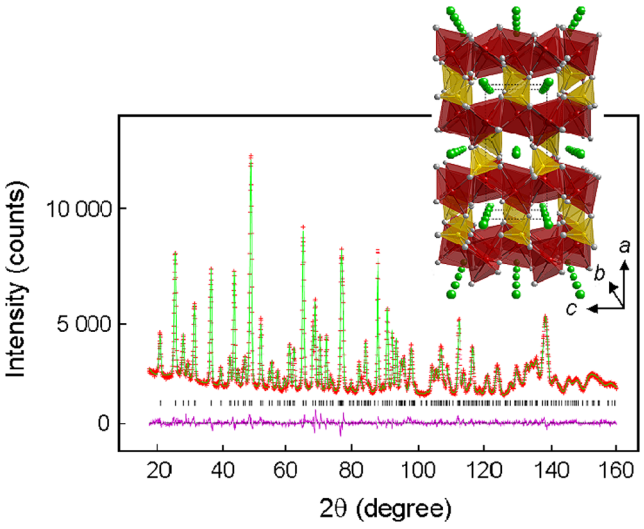

FIG. 1 (color online). Neutron powder diffraction data and their Rietveld refinement pattern for $LiFePO_4$ annealed at 600 °C for 5 h. The observed intensity data are represented by red (or gray) plus (+) signs, and the green (or light green) solid line overlying them is the calculated intensity. Differences between the observed and the calculated intensities are plotted underneath in pink (or gray). Vertical tick (|) signs above the differences indicate the Bragg reflection positions. The inset is a crystal structure of $LiFePO_4$ shown perpendicular to the b axis, illustrating a well-ordered cation partitioning between Li and Fe; Li [green (or light gray)] in the $M1$ octahedron and Fe [red (or gray)] in the $M2$ octahedron. Phosphorus [yellow (or lightest gray)] is located in the tetrahedral site, forming a polyanion with four oxygen (gray) atoms, $[PO_4]^{3-}$.

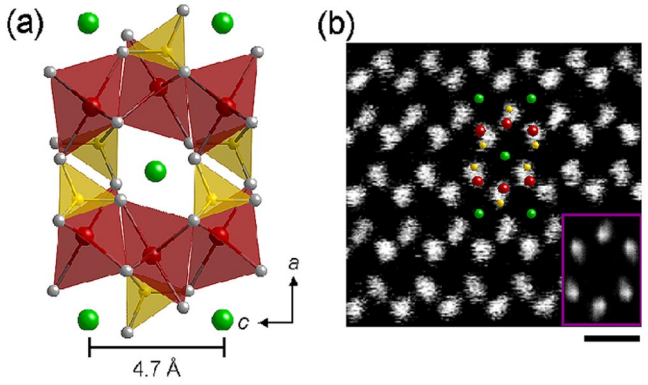

FIG. 2 (color online). Illustration of the atomic configuration in a unit cell of $LiFePO_4$ and HAADF-STEM image. (a) The schematic for the [010] projection represents an ordered arrangement of Li [green (or light gray)] and Fe [red (or gray)]. In this projection, the phosphorus [yellow (or lightest gray)] tetrahedron appears to be much closer to the Fe octahedron than it is in three-dimensional real space. (b) The Z-contrast STEM image of the [010] projection directly demonstrates the ordered atom columns for Fe-P as bright features. The Li columns are invisible due to the low atomic number of Li. The superimposed atomic array on this image compares the locations of each atom. The inset indicates a simulated ADF image, consistent with the experimentally obtained image. The scale bar is 5 Å.

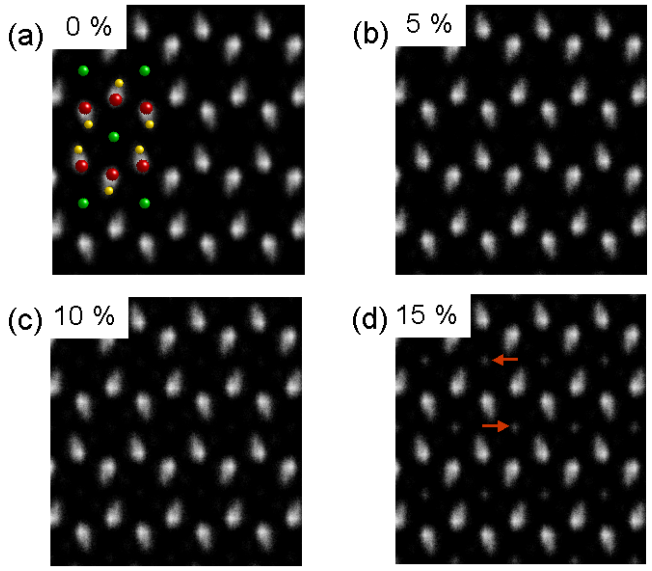

FIG. 3 (color online). A series of simulated ADF images as a function of the degree of disordering between the M sites. The intensities in each image are calculated for (a) 0%, (b) 5%, (c) 10%, and (d) 15% Li-Fe exchanges. The Li columns show a sufficiently bright intensity to be recognized at 15% exchange, whereas the contrast in the Fe columns hardly varies with the exchange.

Fe and P columns are not obviously discriminated, but are instead represented as an oval-shaped single feature in our case, consistent with the simulated image shown in the inset.

To compare the contrast variations by the M-site exchange quantitatively, we carried out image simulations as a function of the degree of exchange. Figure 3 shows a series of simulated images in the [010] projection when the degree of Li-Fe exchange hypothetically varies up to 15% at each M site. While no detectable variation in intensity is observed in the Fe columns for the exchange, it is noted that the Li columns show a visible white contrast when a 15% Li-Fe exchange occurs at each octahedral site, as indicated by a red (or gray) arrow in Fig. 3(d). The actual intensity of an atom column is dependent on the average Z^2 of each atom if the column consists of different atoms [17]. In this regard, unlike for the Li columns, the insensitive change in contrast for the Fe columns is not surprising because just a small portion (15%) of much heavier Fe atoms are replaced with lighter Li atoms.

The b lattice constant for $LiFePO_4$ is ~6 Å, and two Li atoms are located in the unit cell through the Li column along the b axis, as shown in the inset of Fig. 1. If the specimen thickness is assumed to be ~12 nm, the scanned region during the STEM can be estimated to contain 20 unit cells in the [010] projection, indicating that 40 Li atoms are included in every Li column. Therefore, the simulation result shown in Fig. 3 demonstrates that the occupation by six Fe atoms (~15% of 40) in each Li column can make the column visible with sufficient intensity when a thin specimen is used as it was in this study.

During the STEM analysis, we critically observed HAADF images showing a detectable intensity in some of the Li columns for the sample annealed at 600 °C, whereas such a Li-to-Fe exchange contrast was scarcely found in the sample annealed at 800 °C. Figure 4(a) illustrates a raw HAADF image and its magnified parts that reveal a visible Z contrast for some of the Li columns in the 600 °C sample [red (or gray) arrows], directly indicating that Fe atoms occupy the Li sites as antisite defects. These images were captured for a typical region with the defects

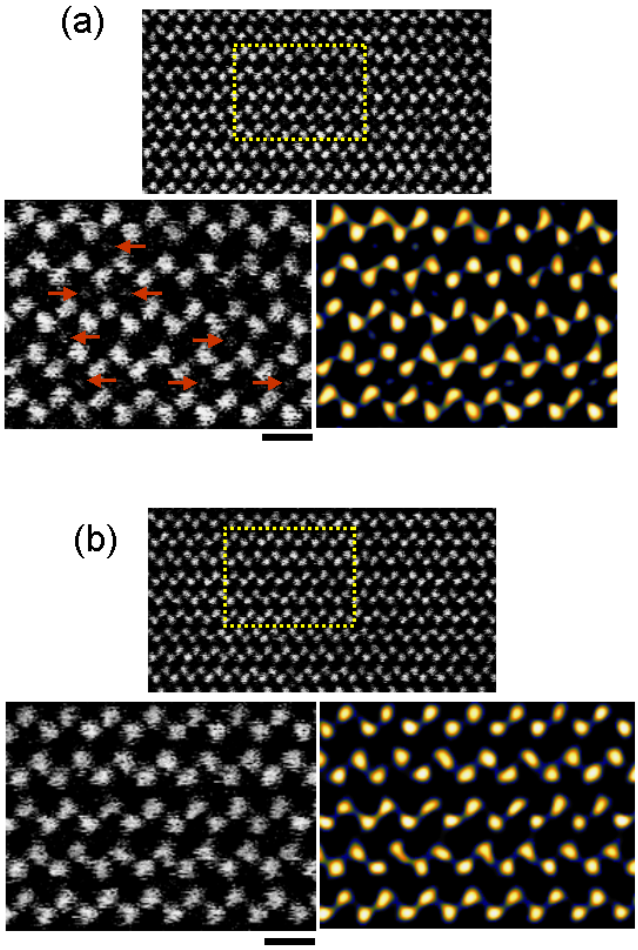

FIG. 4 (color online). HAADF-STEM images and their magnified images for each region denoted by a yellow (or light gray) rectangle for $LiFePO_4$ crystals with a [010] zone. (a) The enlarged images clearly show that some of the Li columns have a bright contrast in significant intensity for a sample annealed at 600 °C [red (or gray) arrows] while maintaining the ordered arrangement of the Fe-P contours. (b) No Li columns with visible intensity are observed when annealing at 800 °C. Such a high degree of ordering in the Li sites is in good agreement with the neutron diffraction result. Each corresponding deconvoluted image is provided in color (shading) on the right, respectively. The scale bars are 5 Å.

so as to show that the visible columns were locally aggregated, although the ordered framework is maintained quite well in many of the observed regions, as shown in Fig. S2 in the supplementary information [16]. By contrast, any visible intensity in the Li columns was hardly found for the 800 °C sample, as represented in Fig. 4(b) and more clearly in the magnified images. To clarify that the bright contrast of the visible Li columns does not originate from the background noise by the electron probe function, a deconvolution processing [18] was carried out with the raw HAADF images [19]. Each deconvoluted image corresponding to the region denoted by a yellow (or lightest gray) rectangle is also shown in color (shading) on the right in Figs. 4(a) and 4(b), respectively, confirming the antisite defects on the Li columns consistently. An additional image comparison for more information is provided in Fig. S3 in the supplementary information [16].

It should be noted that invisible contrast in the Li columns does not always mean the absence of the exchange defects in the lattice, as demonstrated in the image simulation of Fig. 3. However, recalling that the overall M site exchange between the Li and Fe sites for the 600 °C sample is as slight as just $\sim 1\%$ based on the neutron diffraction result, such a remarkable variation in the HAADF images shown in Fig. 4(a) viably suggests that the exchange defects in the Li sites are localized at a lower temperature rather than to be homogeneously distributed in the lattice.

The $M1$ sites in the olivine structure are edge-sharing octahedral interstitials, as described above. Thus, the distance between the neighboring cations in the $M1$ sites is shorter than that in the corner-sharing $M2$ sites [15]. Such a structural configuration leads to the distorted shape of the oxygen octahedra for the $M1$ sites to minimize the electrostatic repulsion between the cations [15]. If some of Fe^{2+} ions occupy the $M1$ sites instead of Li^{+} in $LiFePO_4$, additional electrostatic repulsion due to their higher valence number can be induced, eventually resulting in a structural instability. In this regard, we do not expect that the local aggregation of disordered Fe in the Li sites would be thermodynamically favorable. It can be deduced therefore that the aggregation may be reduced by annealing at a higher temperature or for a longer enough period of time.

Although the Fe-P contours in the HAADF images are insensitive to the exchange by Li atoms, we have observed a few Fe-P contours with fairly low intensities during the STEM, as exemplified in Fig. S4 in the supplementary information [16]. Because associated Fe vacancies may contribute to the low intensity in addition to the exchange by Li in this case, it will not be simple to determine whether or not the exchange defects are localized in the case of the Fe sites. Further complementary analyses are necessary to precisely address the distribution of the disordered Li atoms occupied in the Fe sites.

In summary, we have directly demonstrated the disordered occupations by Fe atoms on Li sites in $LiFePO_4$ with an ordered olivine structure, using HAADF-STEM. Such exchange defects appear to be locally clustered in the lattice at a relatively low temperature, although their overall concentration is fairly low. The HAADF-STEM with the corrected spherical aberration can be extensively used as a powerful methodological tool for understanding the atomic-level distribution of point defects.

We thank W.-B. Im at KAIST for assistance with the neutron diffraction analysis and Y.-M. Kim and Y.-J. Kim at KBSI for fruitful discussion on the crystallography of olivines. This work was supported by the Korea Research Foundation, Grant No. 2006-311-D00570. One of the authors (S.-Y. C.) also acknowledges the financial support from the Korea Science and Engineering Foundation, Grant No. R01-2006-000-10765-0.

*Corresponding author.
nalphates@gmail.com; sychung@inha.ac.kr
†Corresponding author.
youngchoi@kims.re.kr

[1] G. R. Helffrich and B. J. Wood, Nature (London) **412**, 501 (2001).
[2] R. N. Schock *et al.*, J. Geophys. Res. **94**, 5829 (1989).
[3] L. M. Hirsch and T. J. Shankland, Geophys. J. Int. **114**, 21 (1993).
[4] J. J. Papike and M. Cameron, Rev. Geophys. Space Phys. **14**, 37 (1976).
[5] C. M. B. Henderson *et al.*, Science **271**, 1713 (1996).
[6] P. D. Nellist and S. J. Pennycook, Phys. Rev. Lett. **81**, 4156 (1998).
[7] P. E. Batson *et al.*, Nature (London) **418**, 617 (2002).
[8] P. M. Voyles *et al.*, Nature (London) **416**, 826 (2002).
[9] U. Kaiser *et al.*, Nat. Mater. **1**, 102 (2002).
[10] P. D. Nellist *et al.*, Science **305**, 1741 (2004).
[11] S. Wang *et al.*, Nat. Mater. **3**, 143 (2004).
[12] J. P. Buban *et al.*, Science **311**, 212 (2006).
[13] Y. Sato *et al.*, Phys. Rev. Lett. **97**, 106802 (2006).
[14] S.-Y. Chung *et al.*, Nat. Mater. **1**, 123 (2002).
[15] A. K. Padhi *et al.*, J. Electrochem. Soc. **144**, 1188 (1997).
[16] See EPAPS Document No. E-PRLTAO-100-074813 for results of neutron diffraction analysis and additional STEM images. For more information on EPAPS, see http://www.aip.org/pubservs/epaps.html.
[17] D. E. Jesson and S. J. Pennycook, Proc. R. Soc. A **441**, 261 (1993).
[18] K. Watanabe *et al.*, Ultramicroscopy **92**, 191 (2002).
[19] The deconvolution of STEM images was done using "DECONVHAADF" (HREM Research, Inc., Japan).